Heat Transfer in Energy Conservation

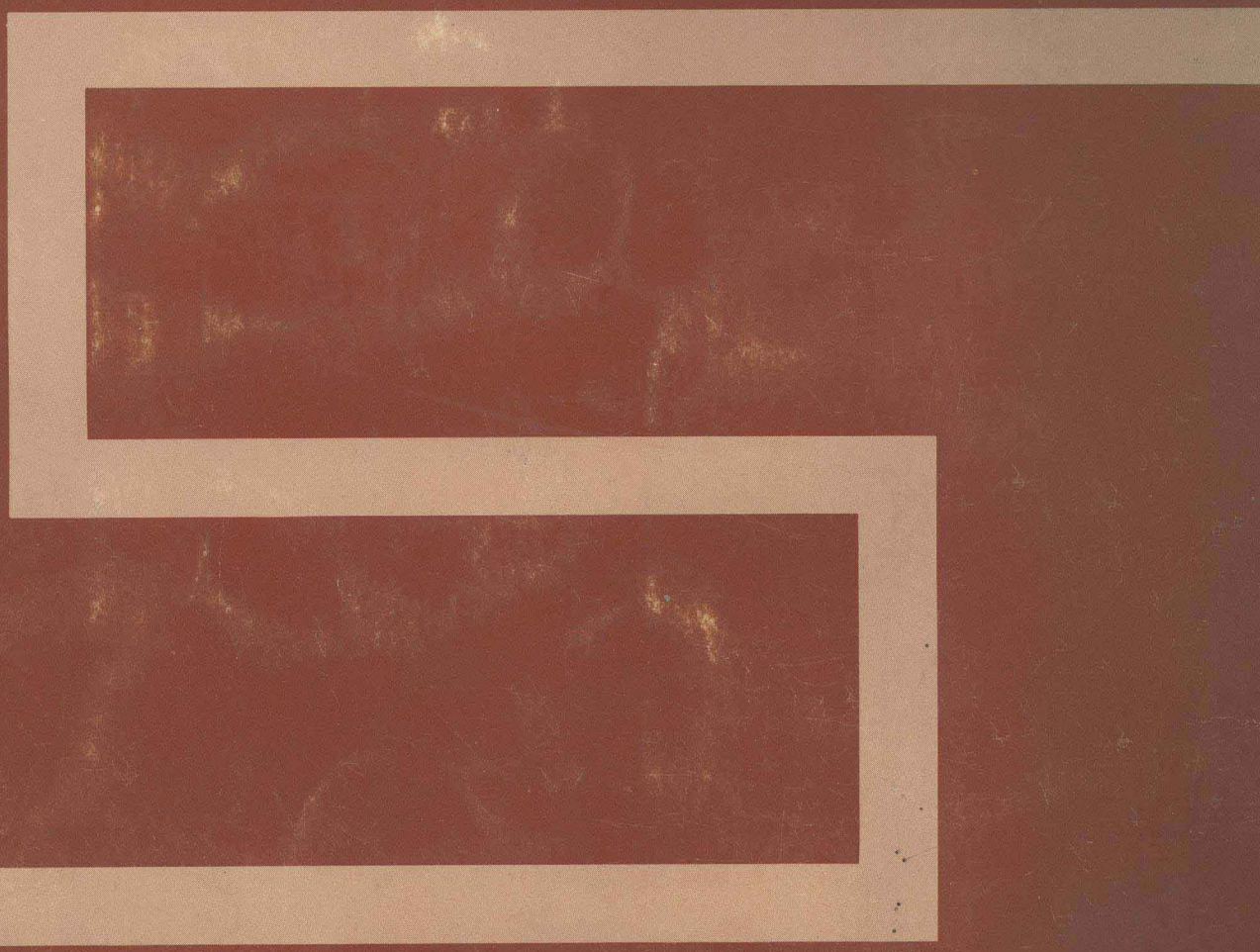

Heat Transfer in Energy Conservation

presented at

THE WINTER ANNUAL MEETING OF
THE AMERICAN SOCIETY OF MECHANICAL ENGINEERS
ATLANTA, GEORGIA
NOVEMBER 27-DECEMBER 2, 1977

sponsored by

THE HEAT TRANSFER DIVISION, ASME
THE ENERGETICS DIVISION, ASME

edited by

R. J. GOLDSTEIN
UNIVERSITY OF MINNESOTA

D. DIDION
NATIONAL BUREAU OF STANDARDS

R. GOPAL
JOHNSON CONTROLS, INC.

K. KREIDER
NATIONAL BUREAU OF STANDARDS

R. SCHOENHALS
PURDUE UNIVERSITY

THE AMERICAN SOCIETY OF MECHANICAL ENGINEERS
United Engineering Center 345 East 47th Street New York, N. Y. 10017

Library of Congress Catalog Card Number 77-87998

STATEMENT from By-Laws. The Society shall not be responsible for statements or opinions advanced in papers or . . . printed in its publications (B7, Par. 3).

PREFACE

The impact of dwindling energy supplies and increasing energy consumption is evident in a number of efforts on the part of the Engineering community. Of particular concern is a long term balance of the use and production of energy resources. A key effort in this regard is conservation without decreasing the "quality of life."

The potential for improvement in our use of energy supplies leads to interest in a number of technological problems related to energy conservation. Evaluation of these problems often requires heat transfer analysis through either known relationships or the development of new basic and applied knowledge. Development of new techniques for measurement of quantities related to heat loss and energy use and monitoring and control instrumentation can also play major roles in improving the efficiency of our energy systems.

Many of the areas related to heat transfer in energy conservation systems are discussed in the papers contained in this volume. These works will hopefully take their place in the community of literature on heat transfer and energy conservation and play a role in reducing our dependence on scarce energy supplies.

The editors would like to express their appreciation for the support of the Heat Transfer Division and the Energetics Division. In particular, the interest of the Chairperson of the Energy sub-committee, C. Tien, and the Heat Transfer Chairpersons, V. Schrock and E. Fried and program representative F. Schmidt were most encouraging. Thanks also to J. Chi and M. Modest who helped formulate the plan for these sessions and aided in bringing them to fruition.

R. J. Goldstein
D. Didion
R. Gopal
K. Kreider
R. Schoenhals

CONTENTS

An Approach to the Digital Simulation of Room Dynamic Thermal Performance Using Thermal Circuit Techniques
Jude R. Anders 1
Multi Space Thermal Coupling Algorithm of the DEROB System
Francisco Arumi 9
Effect of Interior Partitions and Thermal Mass in Modeling Small Homes With an Hour-by-Hour Computer Program
R. S. Dougall and R. G. Goldthwait 17
Potential Energy Savings in Commercial/Residential Communities Based on Integrated Systems Design
Robert E. Holtz and Thomas J. Marciniak 27
Infiltration in Residential Structures
J. E. Janssen, J. J. Glatzel, R. H. Torborg and U. Bonne 33
Molten Salt Energy Storage System – A Feasibility Study
B. G. Jones, R. P. Roy and R. W. Bohl. 39
Air Infiltration in Buildings Due to Wind Pressures Including Some Neighboring Body Effects
W. J. Kelnhofer. 47
Energy Conservation Through Enthalpy Evaluation
Dennis E. Miller, Ramesh Krishnaiyer and Richard N. Laakaniemi 57
Energy Savings Potential of HVAC Air-To-Air Heat Recovery Exchangers
Harry J. Sauer, Jr. and Ronald H. Howell. 65
Total System Consideration for Design of Building's Envelopes
Gideon Shavit. 75
Heat Transfer Effects in Compressed Air Energy Storage
Kirby G. Vosburgh and Philip G. Kosky. 83
Computer Simulation of Water Heater Standby Loss
C. A. Wan 91
Heat Storage in the Ground Mass Surrounding Deep Dry Wells
Leonard Y. Cooper 99
Cycles for Electric Energy Conversion from Low-Temperature Energy Sources
R. P. Shah 107
Optimal System Configuration Total Energy Analysis for a Large Military Installation
F. R. Best, S. B. Goldman and M. W. Golay 113
Energy Conservation Through Technology in Comfort Cooling
Geza S. Farkas 121
Fluidics – A New Potential for Energy Conservation by Continuous High Temperature Monitoring and Control
Tadeusz M. Drzewiecki, R. Michael Phillippi and Charles E. Paras. 127

AN APPROACH TO THE DIGITAL SIMULATION OF ROOM DYNAMIC THERMAL PERFORMANCE USING THERMAL CIRCUIT TECHNIQUES

Jude R. Anders
Senior Research Engineer
Johnson Controls, Inc.
Milwaukee, Wisconsin

ABSTRACT

The application of the thermal/electric circuit analogy to the modeling of room thermal performance has been well established in the literature. The thermal circuit techniques have commonly been applied to those simulations run on an analog computer or where the electric circuit is actually constructed. In the present paper these techniques are used to develop a simulation of room thermal performance for operation on a digital computer. While there exists several excellent simulation programs designed for the estimation of building heating and cooling loads, these are generally characterized as rather large computer programs requiring very detailed building data, and are possibly restricted to hourly computations. The simulation developed here is intended for use in the study of the dynamics of control loops applied to building systems. The programming and building data requirements are kept to a minimum, and the computation time interval may be selected arbitrarily. The procedure is demonstrated with a simulation of a series of experiments reported by the National Bureau of Standards. Also, to show the type of output available from the program, a sample application is briefly presented.

NOMENCLATURE

The overbar, '‾' and dot, '·' are used to denote a vector quantity and the derivative with respect to time, respectively. The matrices of vector equations are denoted by the capital letters 'A' through 'P', with "I' denoting the identity matrix. Other uses of these are clear in the context of the describing statements. Additional notations are as follows:

A - Surface Area (m^2)
C - Thermal Capacitance (J/K)
F_e - Emmissivity Factor
F_s - Shape Factor
I_s - Incident Solar Radiation (W)
L - Characteristic Length (m)
$\dot{Q}$ - Heat Flux (W)
S - Ideal Source of Type Specified by a Subscript
T - Temperature (C)
ΔT - Temperature Difference (C)
T_{AV} - Average Temperature (C)
T_o - Outdoor Air Temperature (C)
V - Volume (m^3)

a - Thermal Diffusivity (m^2/hr)
c - Specific Heat (J/kg·K)
f - Excitation Frequency (hr^{-1})
h - Convection Coefficient ($W/m^2 \cdot K$)
h_o - Exterior Convection Coefficient ($W/m^2 \cdot K$)
k - Thermal Conductivity (W/m·K)
ℓ - Thickness of Lumped Material (m)
n,m - Integers
t - Time (s)
wi,zi - Configuration Parameters for Shape Factor Computation

Φ - Transition Matrix
Ψ_C - Convection Conductance Matrix
Ψ_R - Radiation Conductance Matrix
Ω - Thermal Conductance (W/K)

α - Exterior Surface Absorptance
$\bar{\beta}, \bar{\xi}$ - Vectors of Bond Parameters
ε^A - Exponentiation of Matrix A
ρ - Density (kg/m^3)
σ - Stefan Boltzman Constant ($5.6696 \times 10^{-8} W/m^2 \cdot K^4$)
τ - Computation Time Interval (s)
ϕ - Elements of Series Expansion of Φ

INTRODUCTION

With the recent concern for energy use, the techniques for the analysis of building structures and systems have been greatly improved. In particular, simulation programs which treat the building and its systems in great detail, have been developed for the estimation of building heating and cooling loads. Programs AXCESS, E CUBE, NBSLD, NECAP and TRACE (1) are examples. The application of these has already aided the structural and equipment designs of buildings.

The simulation approach developed in the present paper considers building performance for a different purpose. The primary objective here is to develop a simulation which can be used in the study of the dynamics of control loops as applied to building systems. Where the existing programs are generally characterized as rather large computer programs, requiring very detailed building data, and may be restricted to hourly computations, it is desired here that the program and building data requirements be kept to a minimum while allowing for computation intervals of a minute or less.

Simulation based on the thermal/electric circuit analogy has proved to be a versatile approach for conducting dynamic building thermal studies, (2-5). The thermal circuit models have commonly been implemented on an analog computer or by construction of the electric circuit. The formulation of this paper applies the thermal circuit techniques to a digital simulation. In this way, the benefits of the thermal circuit

approach are retained with the additional advantages of digital implementation. For example, the simulation is truly dynamic; many of the model variables are directly available for measurement; modifications of the model are implemented by simply modifying circuit elements; and, model formulation is straightforward since heat flux paths and thermal storage are modeled directly by individual components of the thermal circuit. In addition, the digital implementation allows the model to consist of ideal circuit elements; circuit changes are easily implemented; and, many routines and data bases formulated for the energy analysis programs can be used with slight modifications.

The general organization of the paper is as follows. First, the form of the model is described with the set of assumptions and restrictions placed on the configuration. Only single room configurations are considered in this paper. Given the set of restrictions, the formulation of equations for the model is presented with a method for their solution. Then, to evaluate the accuracy obtainable with the thermal analysis used, a simulation of a set of experiments reported by the National Bureau of Standards, (11,12), is described. The paper concludes with a brief description of an application problem to demonstrate the type of output available.

Thermal Circuit Components

The thermal analysis employed in formulating the room model is quite elementary. The thermal circuit construction is a linear, constant, lumped parameter model of a distributed thermal network. The basic component relations are depicted in Table 1.

Table 1 Basic Thermal Circuit Components

Sources:	$S=S(t)$	
	Temperature	$S_T=T(t)$
	Heat Flux	$S_{\dot{Q}}=\dot{Q}(t)$
Conductance:	$\dot{Q}=\Omega(\Delta T)$	
	Convection	$\Omega=hA$
	Conduction	$\Omega=kA/\ell$
	Radiation	$\Omega=\sigma AF_sF_e(4T_{AV}^3)$
Storage:	$T=1/C\int\dot{Q}dt$	
	Capacitance	$C=V\rho c$

Construction of the room thermal circuit places a conductance for each heat transfer path to be considered, and a capacitance for elements with significant thermal storage. Thermally massive conduction paths (e.g. walls and floors) are modeled by a series of networks where each sub-element of the series models a specified thickness of the path. In order to obtain the desired linear, lumped parameter model, the following simplifications of the thermal analysis are generally employed.

1 Room air is sufficiently mixed to allow for the assignment of a single temperature.

2 Room air is a non-absorbent medium for radiant transfer between elements of the room envelope.

3 Interior surfaces are gray body emitters and absorbers with negligible reflection.

4 Radiant energy leaving a surface has a diffuse directional distribution and uniform magnitude distribution over the surface.

5 Radiant transfer relation is linearized by the approximation $T_1^4-T_2^4\approx(4T_{AV}^3)(T_1-T_2)$.

6 Thermal storers and conductance paths have a uniform temperature distribution on planes perpendicular to the heat flux.

7 Thermally massive conductive paths are partitioned such that the thickness of each partition satisfies the relation $\ell\leq 0.134\sqrt{a/f}$.

The first of these allows a single capacitor model for the interior room air. Simplifications #2-#5 allow radiant transfer between interior room surfaces to be modeled as linear, constant conductances. The approximation, #5, introduces an error of only ten percent when $T_1=2T_2$, (1). The last two set the procedure for lumping of wall and floor models. The rule given in #7 is derived from the lumped approximation of the resistance-capacitance transmission line and results in an error in the heat flux calculation on the order of five percent, (1).

Room Configuration

In order to limit the data requirements and simlify the geometrical computations involved in the determination of radiation shape factors and the manipulation of solar effects, further restrictions are placed on the set of allowable room configurations. The rooms allowed have the form of a right-rectangular parallelopiped where each side of the room envelope may have an arbitrary number of rectangular sub-elements. An example of an allowable room configuration is shown in Figure 1.

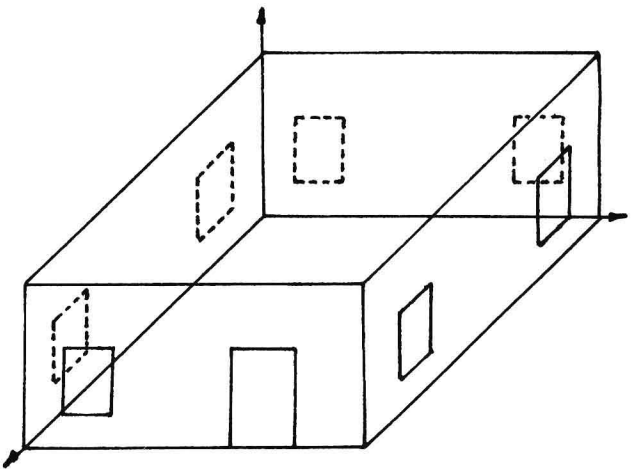

Figure 1 Example Room Configuration

With this form, the sub-elements of the room perimeter can easily be located and described. Also, using the line integral formulation (6), it can be shown that the computation of shape factors between room elements reduces to simple manipulations employing shape factor algebra, (7,8) and a sum of double integrals of the form:

$$\Psi(z1,z2,z3,z4,z5)=\int_{z3}^{z4}dw1\int_{z1}^{z2}\ell n[(w2-w1)^2+z5^2]dw2 \quad (1)$$

THERMAL CIRCUIT STATE EQUATIONS

With the previously specified restrictions on the model, the form of the thermal circuit state differential equations can be described. The circuit is partitioned into an interior radiation and convection network which has a predictable configuration for all rooms from the allowable set; and, a perimenter element network to model the walls, floor, etc. which is constructed according to the specific simulation problem. These are discussed below. The Bond Graph Approach, (9), has been used for formulating the network equations. The diagrams used here are written in the Bond Graph notation. This approach was selected

for the ordering it provides and the clarity with which causality is displayed on the circuit diagram. With this notation, each bond written e.g. '$\overset{1}{\longrightarrow}$' has an associated temperature, (T_1) and heat flux variable $\dot{Q}_1$. Each component of the diagram specifies a relationship between these variables as given in Table 1. The arrow on a bond depicts sign convention, and the bar a dependency or causality relation. A 0-junction has a common temperature at all its bonds and a 1-junction, common heat flux. Conversion to the more conventional electric diagrams can be accomplished by placing a node of the electric circuit at each 0-junction and replacing the 1-junction with a conductance path between the associated nodes. Capacitors are placed from a node to the electrical ground.

Interior Radiation and Convection Network

The interior of the room consists of a conductance network incorporating the convection and radiation heat flux paths. The model restrictions described above result in a predictable pattern for the interior network which depends only on the number of perimeter elements. The network for a four element configuration is shown in Figure 2. Bond 2 of the figure represents the interface to the air capacitance and Bond 1 to an external heat flux which may represent equipment supply. There is one interior

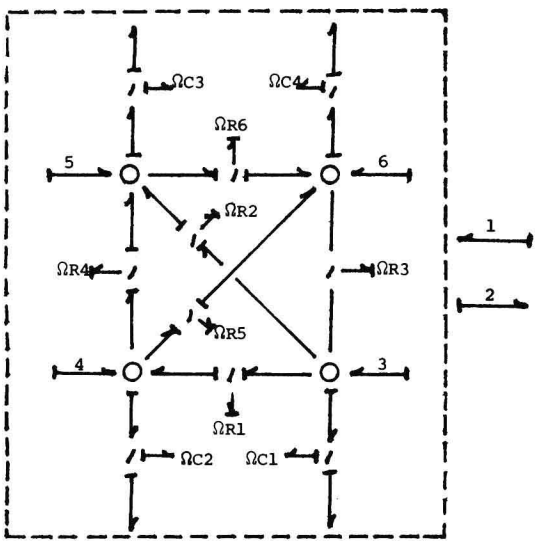

Figure 2 Bond Graph of the Radiation and Convection Network for a 4-Element Configuration (The Outer Box Represents a Single 0-Junction)

0-junction for each room perimeter element, and Bonds 3 to 6 represent the interface to the perimeter element circuit models. The conductances shown depict the convection (ΩC) and radiation (ΩR) heat flux paths. A similar diagram can be drawn for a room with n-elements, and, following the bond graph procedures, (8), an input/output relation for the interior network is obtained as:

$$\bar{\xi}=G\bar{\beta} \tag{2}$$

where $\bar{\xi}$ and $\bar{\beta}$ contain only the perimeter element bond parameters:

$$\bar{\xi}=\begin{bmatrix} T_1 \\ \dot{Q}_2 \\ T_3 \\ \vdots \\ T_{n+2} \end{bmatrix} \qquad \bar{\beta}=\begin{bmatrix} \dot{Q}_1 \\ T_2 \\ \dot{Q}_3 \\ \vdots \\ \dot{Q}_{n+2} \end{bmatrix} \tag{3}$$

and the (n+2)x(n+2) matrix G is written as:

$$G=\left[\begin{array}{cc|ccc} 0 & 1 & 0 & \cdots & 0 \\ 1 & 0 & 1 & \cdots & 1 \\ \hline 0 & 1 & & & \\ \vdots & \vdots & & [\Psi C+\Psi R]^{-1} & \\ 0 & 0 & & & \end{array}\right] \tag{4}$$

The nxn matrix ΨC is a diagonal matrix with the convection conductances as the diagnonal entries. The nxn matrix ΨR has off-diagonal entries in the i-th row given by the ordered and negated radiation conductances joined to the i+2 element node. The i-th diagonal element is the absolute value of the sum of the other i-th row entries. For the network shown in Figure 2, these matrices are written as follows:

$$\Psi C=\begin{bmatrix} \Omega C1 & 0 & 0 & 0 \\ 0 & \Omega C2 & 0 & 0 \\ 0 & 0 & \Omega C3 & 0 \\ 0 & 0 & 0 & \Omega C4 \end{bmatrix} \tag{5}$$

$$\Psi R=\begin{bmatrix} \Omega R1+\Omega R2+\Omega R3 & -\Omega R1 & -\Omega R2 & -\Omega R3 \\ -\Omega R1 & \Omega R1+\Omega R4+\Omega R5 & -\Omega R4 & -\Omega R5 \\ -\Omega R2 & -\Omega R4 & \Omega R2+\Omega R4+\Omega R6 & -\Omega R6 \\ -\Omega R3 & -\Omega R5 & -\Omega R6 & \Omega R3+\Omega R5+\Omega R6 \end{bmatrix} \tag{6}$$

The relationship (2) couples the individual perimeter element models which are considered next.

Perimeter Element Models

The perimeter element models are interfaced to the radiation and convection network at the free bonds previously indicated, e.g. bonds 3 to 6 of Figure 2. These elements, walls, windows, interior room mass, etc are modeled by lumped linear equations. The detail of the model is determined by the specific simulation problem, according to the rules cited earlier. For example, Figure 3 shows a simple exterior wall model with a sol-air temperature source for exterior conditions. In Figure 4 the exterior conditions are presented in more detail, including dry bulb temperature, incident solar radiation, and equivalent temperature of the surroundings.

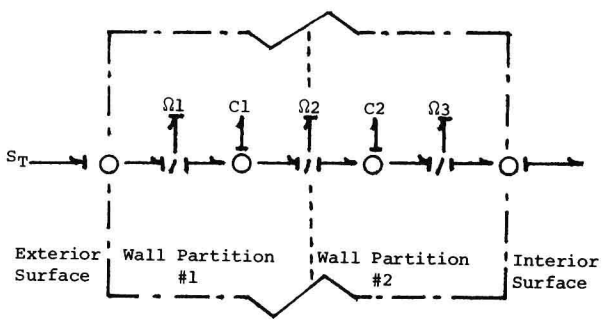

Figure 3 Simple Wall Model With Sol-Air Source S_T
$S_T=T_o+\alpha I_S/h_o$

For each of the perimeter elements a set of state differential equations can be written. Similarly, an equation is written for the air node, Bond 2 of Figure 2, and for the heat flux at Bond 1 of Figure 2. These can be combined to form the matrix relations.

$$\dot{\bar{Q}}=A\bar{Q}+B\bar{\xi}+C\bar{S} \tag{7}$$

$$\bar{\beta}=D\bar{Q}+E\xi+F\bar{S} \tag{8}$$

Using (2) the vector $\bar{\xi}$ can be eliminated to yield:

$$\dot{\bar{Q}}=H\bar{Q}+K\bar{S} \tag{9}$$

$$\bar{\beta}=L\bar{Q}+M\bar{S} \tag{10}$$

where: $H=A+BG(I-EG)^{-1}D$
$K=C+BG(I-EG)^{-1}F$
$L=(I-EG)^{-1}D$
$M=(I-EG)^{-1}F$

Equations (9) and (10) constitute a set of state differential equations for the room thermal model. These could be used directly for simulation of the room through use of some form of integration routine. However, the approach taken here is to solve the equations and apply the results to the room simulation.

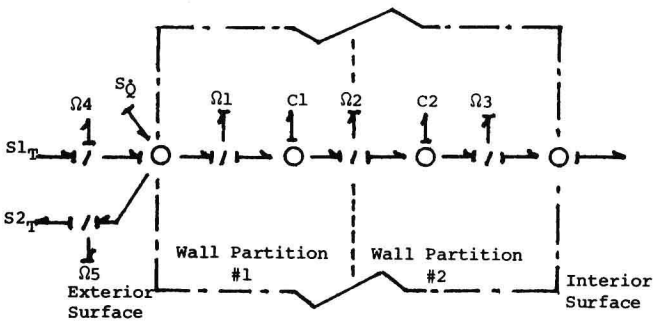

Figure 4 Wall Model With Detailed Exterior Conditions
$S_{\dot{Q}}$ - Absorbed Solar Radiation
$S1_T$ - Outdoor Dry Bulb Temperature
$S2_T$ - Equivalent Temperature of the Surroundings

State Difference Equation Set

The state differential equations can be integrated by computing the transition matrix for a specified time period τ,

$$\Phi(\tau)=\epsilon^{H\tau} \tag{11}$$

An accelerated time series method, (10) is used to compute $\Phi(\tau)$ and is described by the relations:

$$\Phi(t)=\sum_{n=0}^{\infty}\phi_n \tag{12}$$

$$\phi_o=I \tag{13}$$

$$\phi_{n+1}=(t/n+1)H\phi_n \tag{14}$$

$$\tau=2^m t \tag{15}$$

$$\Phi(\tau)=\Phi(2^m t)=\Phi^m(t) \tag{16}$$

The constant m is used to accelerate the convergence of the series (12) and the computation is terminated by satisfying a relation on the norm of the last term, as described by Bierman (10).

The input matrix of the difference equation set can be computed as (11):

$$P=H^{-1}(\Phi(\tau)-I)K \tag{17}$$

and the complete set of equations for the room model can be written for discrete times in increments of τ as:

$$\bar{Q}[(k+1)\tau]=0\bar{Q}(k\tau)+P\bar{S}(k\tau) \tag{18}$$

$$\bar{\beta}(k\tau)=L\bar{Q}(k\tau)+M\bar{S}(k\tau) \tag{19}$$

$$\bar{\xi}(k\tau)=G\bar{\beta}(k\tau) \tag{20}$$

where: $0=\Phi(\tau)$; k=0, 1, 2,...

These equations form the simulation of the room model. The simulation routine itself consists of computing the values of the sources, $\bar{S}(k\tau)$, and the difference equations (18-20) to move the simulation through time at discrete time intervals of length τ. Note that this computation also provides many of the key temperatures and heat fluxes of the network model.

At present, the procedures described here have been implemented by a series of programs. The first computes matrix G of (2) from user data consisting of a description of the room configuration and several required constants. The second program requires the non-zero elements of (7) and (8) and matrix G to compute the matrices of (9) and (10), and those of (18). All of the computed matrices are available for use by the simulation program which is the final program. To use the simulation program, a source subroutine must be written to compute $\bar{S}(k\tau)$ as described above. In addition, several simple output routines are required to identify desired output listings and plots.

SIMULATION PROBLEM #1

To evaluate the application of this approach, a simulation of a series of tests conducted by the National Bureau of Standards, (11,12), was developed. Details of the NBS tests are published in the cited references. The building is of masonry construction with outside plan dimensions of 6.1x6.1m (20x20 ft) with 3.05m (10 ft) high walls. Construction details include:

1 Roof Construction - 0.102m (4 in.) thick precast reinforced concrete slab.

2 Wall Construction - 0.203x0.203x0.406m (8x8x16 in.) solid concrete blocks.

3 Floor Construction - 0.051m (2 in.) polystyrene insulation on grade topped by a 0.051m (2 in.) thick concrete slab.

4 Door - 2.01x0.813x0.05m (79x32x2 in.) solid wood door.

5 Windows - 1.02x0.813m (40x32 in.) windows, a toal of seven for those tests with windows.

6 Insulation - 0.051m (2 in.) thick polystyrene applied to walls and roof according to the test.

7 Internal Mass - 1179 kg (2600 lb) of concrete block placed in the room according to test requirements.

The building configuration with windows is shown in Figure 1. It was constructed inside a high-bay environmental laboratory and instrumented. During the tests the laboratory air was controlled through a 24 hour cycle representing a sol-air profile. The building was subjected to a series of floating tests and thermostated tests. For the floating tests, room air temperature was allowed to vary as the laboratory air was controlled over the sol-air profile. During the thermostated tests, room air was controlled by a system of electric fans and heaters. The experimental data obtained from the tests was subjected to harmonic analysis to produce the curves published. Only the floating test simulations are reported here.

The various test building conditions during the floating tests are summarized in Table 2. Room air variations were published for all the tests. Also,

the ceiling, wall, and floor flux were available for test #1.

Table 2 Floating Test Conditions

Test No	Insulation	Windows	Internal Mass
1	None	None	None
2	None	None	Mass
3	None	Single Pane	None
4	Inside	Single Pane	Mass
5	Outside	Single Pane	Mass

The thermal circuit simulation model employed treated the windows and door as simple conductances; the walls and floor (including a 10.152m (6 in.) depth of earth), were lumped into 4 partitions each and the ceiling 3 partitions. Except as noted below, the thermal properties of materials used in the simulation were those suggested by Peavy, Powell and Burch (11). Two sources were used, a sol-air profile, Figure 5, obtained from a Fourier series analysis of the published curve, and a constant temperature source to model the earth beneath the building. Infiltration

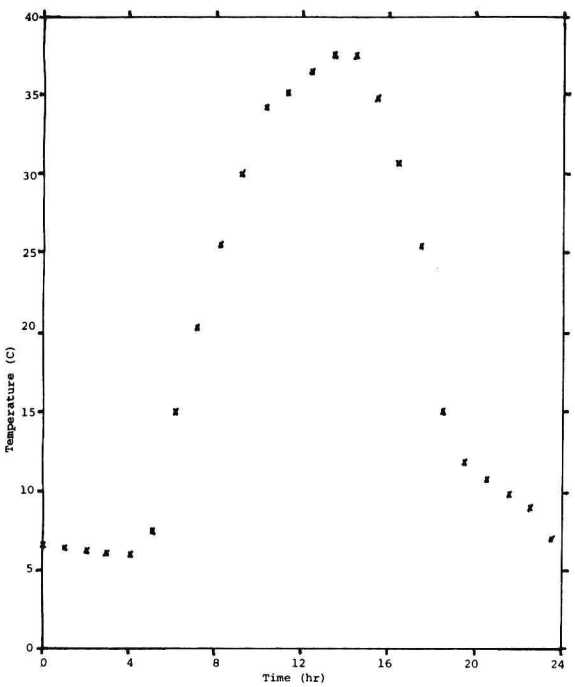

Figure 5 Test #1 Sol-Air Profile

was modeled by a conductance between exterior and interior air. Two methods were used to model the interior mass. The first lumped the mass into a single thermal capacitance connected to the interior air node through a convection conductance. This approach neglected the radiation transfer, and resulted in a slightly more dominant damping effect than displayed by the experimental results. The second technique distributed the mass over the floor. The results reported here are for the second approach.

The floating tests involve only natural convection at both interior and exterior surfaces. The convection coefficients were assumed constant for each test. A value of 8.35 was used for all exterior surfaces for all tests. The interior coefficients were computed for each test as follows:

$$\text{Wall Coefficient: } h=1.312(\Delta T)^{1/3} \tag{21}$$

Floor & Ceiling Coefficients:

$$h=\frac{1}{2}\left[1.52(\Delta T)^{1/3}+0.586\left(\frac{\Delta T}{L}\right)^{1/4}\right] \tag{22}$$

These relations were taken from the ASHRAE Handbook of Fundamentals, (14). Relation (22) is actually an average of the coefficients for the two possibilities of heat flux and surface orientation. The temperature difference used in the relations was determined by running the simulation, observing the average temperature, and recomputing the convection coefficients. This was repeated until the correction in coefficient values was insignificant. The resultant coefficients are shown in Table 3.

Table 3 Interior Convection Coefficients

Test No.	Wall	Floor	Ceiling
1	0.857	1.01	1.19
2	0.863	0.994	1.19
3	1.23	1.08	1.08
4	1.25	0.829	1.15
5	0.948	0.761	0.670

The results of the simulation are shown on Figures 6 thru 13, with the published results of the corresponding NBS tests. In all cases, the fit of simulation data to test results is quite good. The poorest match of room air temperature data is that of tests #4 and #5, Figures 12 and 13, where there is an offset for the entire plot. The insulation used in these tests causes a considerable reduction in conduction across the walls. As a result, the room air temperature variation depends heavily on the conduction across the windows and on infiltration. A more detailed treatment of these could possibly eliminate the offset. With regard to the heat flux plots of test #1, the floor and ceiling plots, Figures 7 and 9 show good correspondence. The largest errors here occur when the heat flux and surface have opposite directions. Apparently, the convection coefficients, which were held constant for the simulation, provide for excessive transfer at the interior surfaces in this case. The effect of the constant coefficients is also seen in the wall flux plot, Figure 8. The authors of the NBS report, (12), relate the irregularity of the wall flux at its peak to the changing directions of both ceiling and floor flux. This change affects the room air flow pattern and consequently, the convection transfer at the walls. The constant coefficients of the simulation program prevent it from demonstrating this occurrence.

SIMULATION PROBLEM #2

A thermal circuit room model was constructed to study the properties of various loops for room air temperature control. To incorporate the control loop in the simulation, the source routine contained computations for a first order sensor model, an error calculation and a control algorithm. The measured variable was room air temperature and the manipulated variable was a heat flux source at Bond 2 of the room thermal circuit. Exterior conditions were taken from weather data tapes and included both temperature and solar effects. Interior load was supplied in terms of an hourly profile.

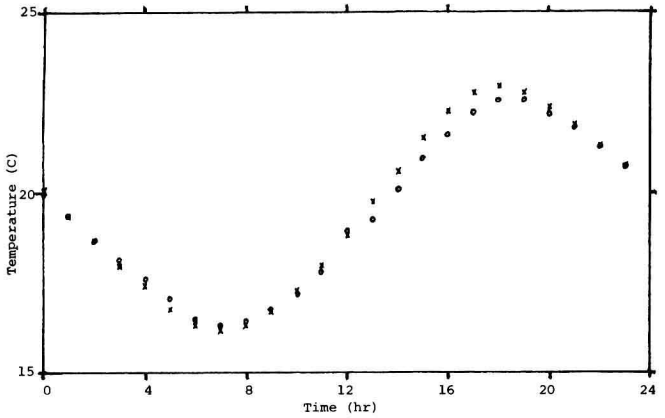

Figure 6 Test #1 Interior Air Temperature
x Thermal Circuit Simulation
o NBS Test Results

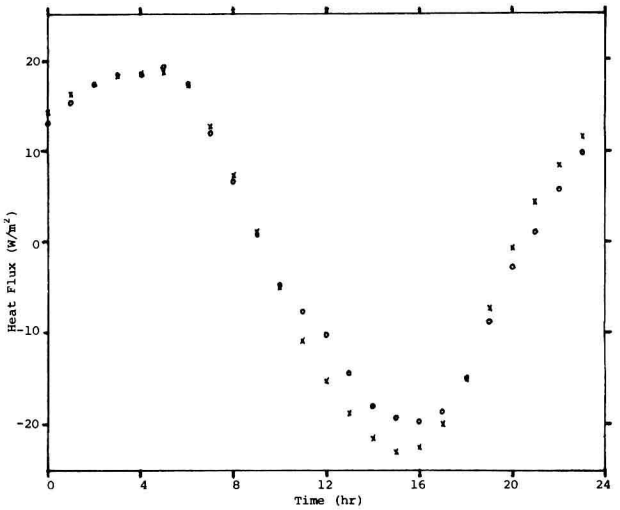

Figure 7 Test #1 Flux at Roof Interior
x Thermal Circuit Simulation

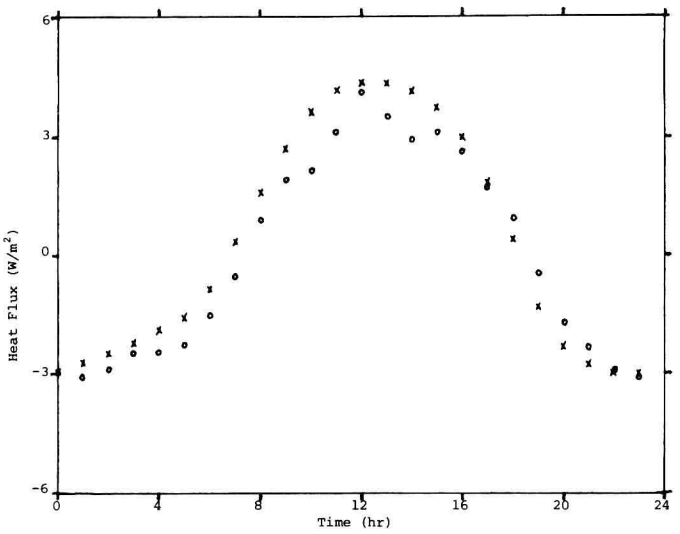

Figure 8 Test #1 Flux at Wall Interior
x Thermal Circuit Simulation
o NBS Test Results

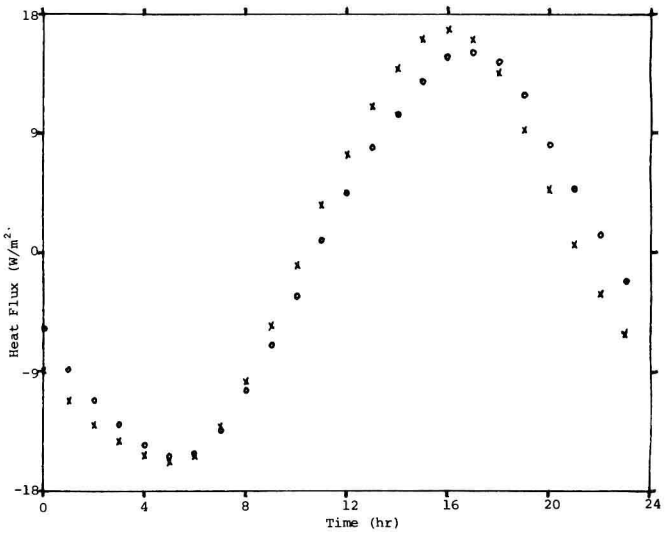

Figure 9 Test #1 Flux at Floor Interior
x Thermal Circuit Simulation
o NBS Test Results

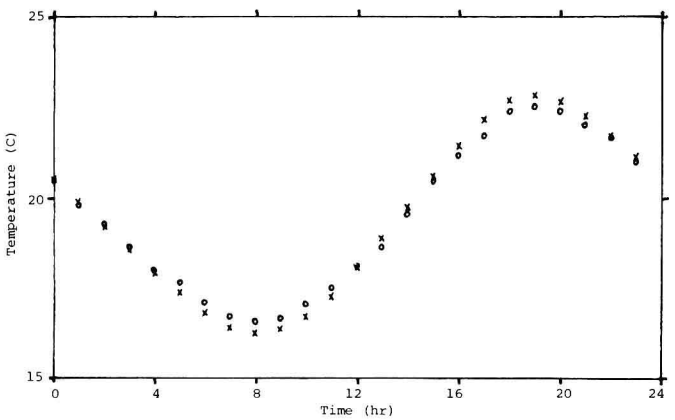

Figure 10 Test #2 Interior Air Temperature
x Thermal Circuit Simulation
o NBS Test Results

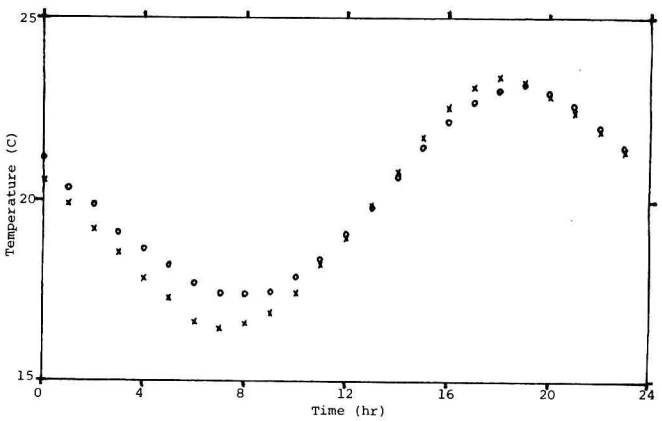

Figure 11 Test #3 Interior Air Temperature
x Thermal Circuit Simulation
o NBS Test Results

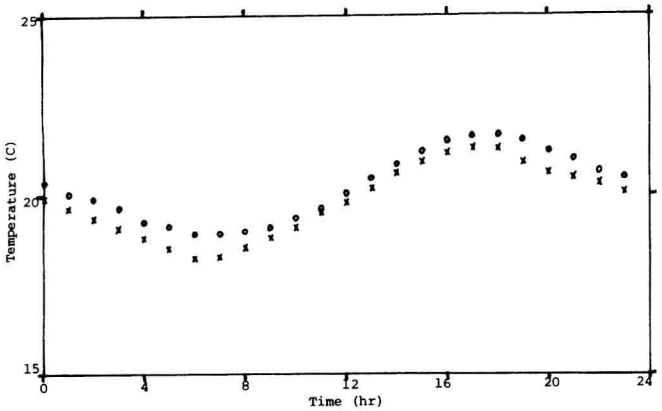

Figure 12 Test #4 Interior Air Temperature
x Thermal Circuit Simulation
o NBS Test Results

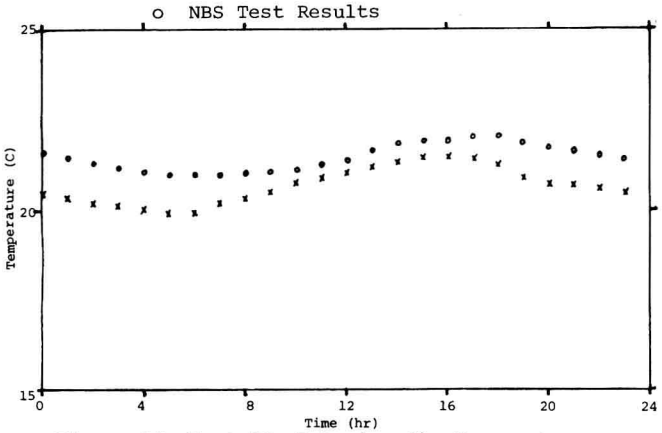

Figure 13 Test #5 Interior Air Temperature
x Thermal Circuit Simulation
o NBS Test Results

A portion of the results of this study is depicted in Figures 14 and 15. Figure 14 demonstrates the effect of controller bandwidth on room air temperature when a proportional position algorithm is employed. As shown in the figure, for a given bandwidth the steady state error, called offset, is determined by the load condition. For the time period shown, the interior load represents the dominant changing load. At each change in interior load, the room air temperature goes through an initial transient and then settles to a new value offset from the setpoint, but within the loop bandwidth. Also, as shown by the several plots, decreasing loop bandwidth, an increase in controller gain, results in tighter control of the air temperature.

A velocity control algorithm sets the rate of change of the manipulated variable proportional to the error. With this algorithm, steady state error or offset is theoretically eliminated. However, in practice a deadband is selected within which the measured variable may vary without corrective action. This is employed to prevent hunting by the control loop. While offset is easily controlled with the velocity algorithm, it tends to be slow to respond to major system upsets. Figure 15 shows the room air temperature response with velocity algorithm control. The room conditions were the same as with the position algorithm of Figure 14. Note that under steady state conditions, the room air temperature is always within the deadband. Plot #1 is the response obtained with a 15 minute time constant sensor, the same as used with the position algorithm. Plot #2 is the response with a two minute time constant sensor, and shows considerably improved response.

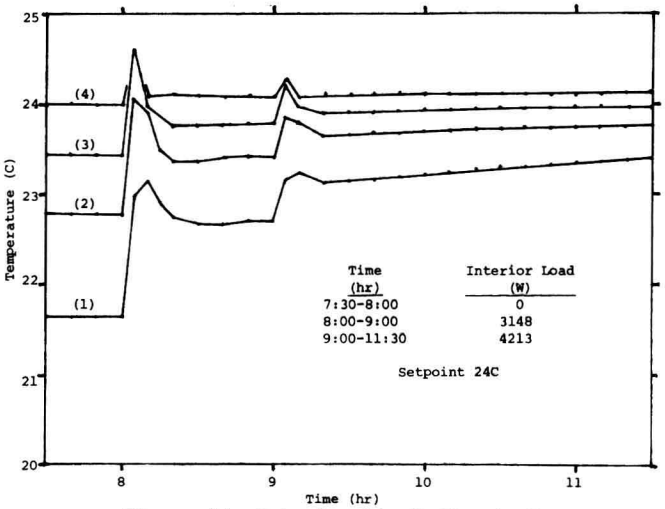

Figure 14 Interior Air Temperature
Proportional Position Control Algorithm
1 4.5C Bandwidth
2 2.2C "
3 1.1C "
4 0.28C "

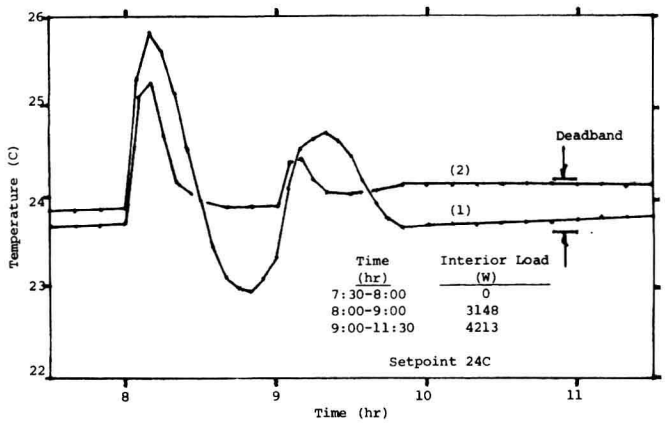

Figure 15 Interior Air Temperature
Proportional Velocity Control Algorithm
1 15 min sensor time constant
2 2 min sensor time constant

The applications discussed here are quite straightforward. The thermal circuit model allows for considerably more detail in the analysis of control loops. Sensor characteristics, non-linearity and hysteresis effects, equipment response, and time lags can all be studied in the environment of a detailed room thermal analysis.

CONCLUSION

A method has been developed and demonstrated which provides for the simulation of room thermal performance on a digital computer. The method employs the thermal/electric circuit analogy to develop a linear constant

set of state difference equations for the room dynamics. As shown by Simulation Problem #1, reasonable accuracy can be expected from the simulation in terms of predicting interior air temperatures, heat fluxes at room elements and phase relationships between the dynamic variables.

The procedure described was developed primarily to study transient behavior of room control loops and for this application its benefits include:

1 Simplicity of problem formulation and consequent ease of modification for study purposes.

2 The simulation maintains close contact with the physical quantities and concepts of the room thermal behavior.

3 The transition matrix soluation to obtain state difference equations provides a stable model of a stable system, ie. stability is not dependent upon sample times and accuracies of a classical integration routine.

4 The procedure can be automated to provide a moderately fast simulation which can run on a small computer.

REFERENCES

1 Chen, Steve Y. S., "Existing Load and Energy Programs," Heating/Piping/Air Conditioning, Dec, 1975, pp 35-39.

2 Nottage, H. B. and Parmelee, G. V., "Circuit Analysis Applied to Load Estimating," ASHRAE Transactions, Vol. 60, 1954, pp. 59-102.

3 Nottage, H. B. and Parmelee, G. V., "Circuit Analysis Applied to Load Estimating, Part II," ASHRAE Transactions, Vo. 61, 1955, pp. 125-150.

4 Buchberg, H., "Electric Analogue Prediction of the Thermal Behavior of an Inhabitable Enclosure," ASHRAE Transactions, Vol. 61, 1955, pp. 339-386.

5 Magnussen, J., "Analog Computer Simulation of an Air Conditioning System in a Commercial Building Incorporating Yearly Weather Data," Use of Computers for Environmental Engineering Related to Buildings, Building Science Series 39, SD Catalog No. C13.29/2:39, U.S. Gov. Printing Office, Washington, DC., Oct, 1971, pp. 146-158.

6 Sparrow, E. M., "A New and Simpler Formulation for Radiative Angle Factors," Transactions of ASME Journal of Heat Transfer, May 1963, pp. 81-88.

7 Sparrow, F. M., "Radiant Interchange Between Surfaces Separated by Non-Absorbing and Non-Emitting Media," Handbook of Heat Transfer, W. M. Rohsenow and J. P. Hartnett, Eds., McGraw-Hill, New York, 1973.

8 Chapman, A. J., Heat Transfer, The MacMillan Co., New York, 1960.

9 Rosenberg, R. C., "State-Space Formulation for Bond Graph Models of Multiport Systems," Transactions of ASME Journal of Dynamic Systems, Measurement and Control, March 1971, pp. 35-40.

10 Bierman, G. J., "Power Series Evaluation of Transition and Co-Variance Matrices," IEEE Transactions on Automatic Controls, Vol. 17, No. 2, April 1972, pp. 228-232.

11 Hansen, R., "Transforming Differential Domans Into Sampled Representations," IEEE Transactions on Automatic Controls, Vol. 19, No. 1, Feb 1974, pp. 61-62.

12 Peavy, B. A., Powell, F. J., and Burch, D. M., "Dynamic Thermal Performance of an Experimental Masonry Building," NBS Building Science Series 45, 1973.

13 Burch, D. M., Peavy, B. A., and Powell, F. J., "Experimental Validation of the NBS Load and Indoor Temperature Prediction Model," ASHRAE Transactions, Vol. 80, 1974, pp. 291-313.

14 ASHRAE Handbook of Fundamentals, New York, American Society of Heating, Refrigeration and Air Conditioning Engineers, 1972.

MULTI SPACE THERMAL COUPLING ALGORITHM OF THE DEROB SYSTEM

Francisco Arumi

Numerical Simulation Laboratory
School of Architecture
University of Texas at Austin
Austin, Texas

ABSTRACT

The physical and mathematical arguments leading to the multi-space thermal coupling algorithm for buildings is given. The radiation balance conditions are coupled to the heat diffusion algorithm for walls, and the walls are in turn coupled to the air through convection. The air among connecting spaces are directly coupled through air exchange which can be either buoyancy induced or forced. The algorithm allows for interaction of the structure with the ground and with neighboring structures. This last feature can be used as an aid in either site planning or environmental impact analysis.

NOMENCLATURE

Letters underlined with one bar stand for vector or first rank arrays. Letters underlined with two bars stand for matrices or second rank arrays.

$\underline{a}$	absorptance vector
A_{li}	the surface area of the lth wall of the ith room
B_k	radiation absorbed per unit of area by surface k
c	specific heat capacity
c_a	specific heat capacity of air
dVi/dt	rate of forced air exchange into ith room
dIi/dt	rate of air infiltration into ith room
dv_{ij}/dt	rate of air exchange between rooms i and j
$\underline{e}j$	the jth base vector
$\underline{\underline{F}}$	generalized illumination tensor
$\underline{F}_i$	driving term of the air temperature of ith room
$\underline{\underline{G}}$	geometric factor tensor (Fij is its i-j component)
h_{li}	film coefficient of the lth wall of the ith room
$\underline{\underline{H}}$	transmittance recursion tensor
$\underline{\underline{I}}$	unit tensor
$\underline{\underline{J}}$	reflectance illumination tensor
$\underline{\underline{k}}$	heat conductivity
L	thickness of wall
n	number of spaces
$\underline{\underline{P}}'$	second coupling tensor
$\underline{\underline{P}}$	reflectance geometric tensor
$\underline{Q}_i$	rate of internal heat generation in room i
$Q_{net}^{(i)}$	rate of net heat lost (gain) in room i
$\underline{\underline{R}}$	first coupling tensor
$\underline{r}$	reflectance vector
$\underline{S}$	source vector
$\underline{\underline{S}}$	reflectance series tensor
$\underline{T}$	air temperature vector (T_i temperature of ith room)
T_{li}	surface temperature of lth surface of ith room
T_{ci}	duct air temperature as it comes into ith room
T_o	outside air temperature
t	time
$\underline{t}$	transmittance vector
$\underline{U}$	a vector with all components equal to 1
V_i	volume of ith room
Δt	increament in time
δ_{ij}	kronecker delta
γ	thermal inertia index
ρ	density
ρ_a	density of air
ω	frequency of thermal environment
ω_i	relaxation rate of air temperature of ith room
ω_{ij}	relaxation rate of the air coupling between rooms i and j

INTRODUCTION

Although many of the limitations pointed out by Mitalas in 1965 (1) of the common assumptions in the calculations of energy consumption in buildings are still present today, considerable improvements have taken place. This is particularly true in the computerized methods that have been developed since then.

The most commonly accepted reference of excellence in this field is the NBSLD program developed by Kusuda (2) in the National Bureau of Standards. Efforts to expand and improve this and other programs continue. One of the areas where these efforts are concentrated (3) deal with the thermal coupling algorithms

This article describes the physical basis of the thermal coupling logic of the DEROB system of programs. Without attempting to give a complete description of the system, this article outlines the organization of the programs. The bulk of the article describes the multi-space thermal coupling. Special emphasis is given to the coupling of the radiation field to the building geometry. The manner in which the radiation equilibrium is

coupled to the energy balance of the heat conducting surfaces is described, as is the convection coupling of these surfaces to the air in the spaces; and the mixing of the air of connected spaces by forced or natural air circulation.

The algorithm to account for specular reflections is also described.[1]

MULTI-SPACE COUPLING

The multi-space coupling requires the simultaneous solution of the instantaneous temperature and heat loads in all the spaces that constitute the test building. The air of the various spaces are coupled whenever air exchange takes place either by thermal bouyancy or forced circulation. First neighbor spaces are coupled by radiaton balance requirements and by natural convection. In addition, if party walls either have openings or windows, adjacent spaces are also coupled by direct radiation. The coupling strength of these mechanisms decreases according to the sequence in which they are mentioned above. The potentially important effects of air mixing and stratification within a space are not accounted for in these algorithms.

Preliminary calculations show (4) (Arumi 1977) that air mixing can be a significant factor in load calculations whenever the heat sources are out of phase; their importance, however, decrease as the rate of forced circulation increases. The two extreme limits of zero and infinite mixing rates can be simulated with the present form of DEROB. The infinite mixing rate is automatically built into this and other thermodynamic models (2) (Kusuda 1974) when the air temperature of a room is assumed to be uniform. The opposite limit can be simulated by disengaging the geometric coupling logic. This version of DEROB is found in the program WALGLAS.

Air Temperature

The rate of air temperature change in any one room is given by:

$$\frac{d}{dt} T_i = \frac{1}{\rho_a c_a V_i} Q_{net}^{(i)} \qquad (1)$$

where the net heat gained is made up of the following additive components:

1. $\sum_{\ell} h_{ei} A_{li} (T_{li} - T_i)$: rate of heat transfer by convection from the wall surfaces. The sum is carried overall the walls facing room i.
2. $\rho_a c_a \frac{dVi}{dt}(T_e - T_i)$: rate of heat transfer by mixing with the air that comes through the ducts
3. $\rho_a c_a$ dI/dt $(T_o - T_i)$: rate of heat transfer by mixing with the air that infiltrates.
4. $\rho_a c_a \sum_j$ dVij/dt $(T_j - T_i)$: rate of heat transfer with air coming from other chambers.
5. Q_i rate of internal heat generation.[2]

Equation 1 can be rewritten in the form:

$$\frac{dT_i}{dt} + \omega_i T_i = F_i + \sum_j \omega_{ij} T_j \qquad (2)$$

where:

$$\omega_i = \frac{(\sum_{\ell} h_{\ell} A_{\ell})}{\rho_a c_a V_i} + \frac{1}{V_i}\left(\frac{dV_i}{dt} + \frac{dI_i}{dt}\right)$$

$$F_i = \frac{\sum_{\ell} h_{\ell} A_{\ell} T_{\ell}}{\rho_a c_a V_i} + \frac{1}{V_i}\left(\frac{dV_i}{dt} T_{ci} + \frac{dI_i}{dt} T_o + \frac{Q_i}{\rho_a c_a}\right)$$

$$\omega_{ij} = \frac{1}{V_i} \frac{dV_{ij}}{dt}$$

These equations depend on the surface temperature of the walls, on the rate of air infiltration, on the rate of air exchange among the rooms, and on the duct air temperature all of which are variables that must be solved simultaneously with the room air temperatures.

The simultaneous solution can be carried out by linearizing the above equations and generating a solution matrix. However, the expressions for thermo-buoyancy air circulation (8) are non-linear; and in many conditions the relaxation times (ω_i^{-1}, and ω_{ij}^{-1}) are small compared with any reasonable time mesh size of integration (of the order of 1 hour) thus making the linearized approach impractical.

For these reasons the simultaneous solution used in this algorithm is carried out by

---

1 The Dynamic Energy Response of Buildings (DEROB) system has been under development independently since 1972 at the Numerical Simulation Laboratory of the School of Architecture of the University of Texas at Austin. It was intended to serve as a research, design, and instructional tool, and it has been used extensively in all these capacities.

2 The rate of internal heat generation is one of the most important parameters in determining the energy performance of commercial buildings. Calculations, carried out by this author (5) with DEROB, of the annual energy consumption of buildings for heating and cooling as a function of building volume, parametric on the rate of internal heat generation, shows the existance of optimum building sizes. The optimum building volume is a single value function of the rate of internal heat generation. As such it provides a natural upper limit for annual energy consumption. A value 3700 BTU/ft^3 was determined for Austin, Texas. It also provides a design guideline of one cubic foot of volume for each BTU/hr of internal heat generation. The energy performance value is consistent with the GSA guidelines (6). This approach, however, also provides for a range of up to 50% lower consumption according to the details of architectural design. The required volume for a given range of internal heat generation is consistent with the Build-Code Requirements (7). When the heat generating activities are distributed through the building according to the building internal partitioning, the energy performance can be improved even more. These calculations, however, depend on the air mixing rates and the partitioning effect conclusions need further investigation.

iteration. The argument goes as follows:

Equations 2 are integrated from time t to time t + Δt and we assume that F_i, ω_i, ω_{ij}, and T_j can be treated as constant over that time interval, and equal to the artithmetic average of their values at times t and t+Δt. (Similar to the Crank-Nicholson (9) solution). In this manner equations 2 can be integrated by direct quadrature to yield

$$T_i' = T_i \exp(-\omega_i \Delta t) + \frac{(1-e^{-\omega_i \Delta t})}{\omega_i} \times$$

$$---\{F_i + \sum_j \frac{\omega_{ij}}{2} (T_j + T_j')\} \qquad (3)$$

where the prime and unprimed quantities are the values of times t + Δt and t respectively.

Expression 3 represent a set of n equations for n unknown air temperatures. Their simultaneous solution can be expressed in covariant notation (independent of coordinate systems) as

$$\underline{T}' = \underline{\underline{R}} \cdot \underline{\underline{P}}' \cdot \underline{T} + \underline{\underline{R}} \cdot \underline{S} \qquad (4)$$

where $\underline{T}'$ is the temperature vector whose ith component is the temperature of the ith room, and the other matrices are defined by their components

$$P_{ij}' = \delta_{ij} e^{-\omega_i \Delta t} + (1-e^{-\omega_i \Delta t}) \frac{\omega_{ij}}{2\omega_i}$$

$$R_{ij}^{-1} = \delta_{ij} - (1-e^{-\omega_i \Delta t}) \frac{\omega_{ij}}{2\omega_i}$$

$$S_i = \frac{F_i}{\omega_i} (1-e^{-\omega_i \Delta t})$$

$$\delta_{ij} = \begin{cases} 1 & i = j \\ 0 & i \neq j \end{cases}$$

Equation 4 is then solved by iteration with the expressions for the wall surface temperatures, and the air circulation.

Surface Temperatures

Bookkeeping. The walls and their surfaces are numbered separately but with related indexing systems. Since edge effects are ignored only two surfaces are assigned to each wall; one is called the "outside" and it always has an odd number index, and the other is called the "inside" and it has an even number index. Thus, for wall member m, surface 2m-1 is its outside surface and surface 2m is its inside surface. The volumes, or chambers, are numbered from 1 to n; two extra "volumes" numbered -1 and 0, are also coded to signify respectively ground contact and external air. Each surface is then coded according to the volume into which they face. This code is used to select the corresponding radiation and heat exposure of each surface and thus establish the heat diffussion coupling between neighboring spaces across their party walls.

Energy Balance. The surface temperatures are obtained from the boundary condition that requires energy conservation at the surface [q]= 0. On the air side the contributions include: direct, diffuse, and reflected visible radiation absorbed by the surface; infrared radiation from the atmosphere (10) and surrounding surfaces by the surface; infrared re-radiation from the surface; and convection heat exchange between the air and the surface. On the wall side the only contribution is the heat flowing by conduction at the surface.

This last term is calculated from the solution of the heat diffussion equation.[3] This can be done by a number of methods. The most efficient method now in use is the response factor method using either the Z-transform method (11) or the time expansion series of the Crank-Nicholson solution.

The surface temperature is also dependant on the thermal history of the opposite surface of the wall. This dependance, of course, is accounted for in the solution to the diffusion equation. In this manner rooms sharing a common wall are thermally coupled by heat diffusion through the wall.

RADIATION EQUILIBRIUM

Single Space

When we consider the distribution of the radiation from a surface among neighboring surfaces, the DEROB algorithm classifies the surfaces as either emmitting or receiving. The first objective of this section is to develop the relationships that establish the distribution of radiant energy among a set of surfaces that define an enclosed volume, and the second objective is to establish the equivalent relationship when several rooms are visually coupled either through openings on the opaque walls or through transparent walls such as windows. The starting point is the fundamental property of the geometric factor, also called the form factor or the view factor, or the angle factor. The geometric factor between the "emmitting" surface j and the "receiving" surface i, G_{ij} stands for the fraction of the total radiation emmitted by surface j that is intercepted by surface i. It can be calculated by integrating the solid angle over the two surfaces. Except for geometries with high symmetry the calculation must be done numeri-

[3] In this connection it must be emphasized that the thermal performance of architectural walls must ultimately be measured either by the thermal comfort they provide or by their contribution to the energy consumed in the building. This requires going beyond the static classification of the thermal characteristics of walls (i.e. their conductance or "R-value"). It requires also going beyond the acknowledgement that the dynamic effects can be accounted for by the appropriate use of a correction factor (12). It requires an expanded classification of walls to include their thermal inertia values as well as their conductance (R-values). It requires the performance classification of the walls according to their coupling to external and internal thermal environments (determined by climate and building occupancy) (13) (14) (15) (16).

cally. The calculation of the geometric factors is the single most expensive calculation in the DEROB system; the present version includes a normalizing cloture logic that truncates the calculation. The fundamental property of the geometric factors follows from the principle of energy conservation. In an enclosed volume, the radiation intercepted by all the surfaces must be equal to the radiation emmitted

$$\sum_i G_{ij} = 1 \qquad (5)$$

summed over all surfaces

In covariant form this equation can be written as

$$\underline{U} = \underline{U} \cdot \underline{\underline{G}} \qquad (6)$$

where the vector $\underline{U} = (1, 1, 1, \ldots, 1)$, and G_{ij} is a component of the tensor $\underline{\underline{G}}$. Each surface has a reflectance transmittance and absorptance such that the three values add up to 1. Define the vectors $\underline{r}$, $\underline{t}$, and $\underline{a}$ such that their ith component is reflectance, transmittance and absorptance of the ith surface; therefore

$$\underline{U} = \underline{r} + \underline{t} + \underline{a} \qquad (7)$$

Substitute 7 into 6 and re-arrange

$$\underline{U} = (\underline{a} + \underline{t}) \cdot \underline{\underline{G}} + \underline{r} \cdot \underline{\underline{G}} \qquad (8)$$

Physically this expression states that the total radiation field is made up of two components; the first component represents what has been absorbed or transmitted, and the second what is left after one reflection. The second term can be rewritten in the form

$$\underline{r} \cdot \underline{\underline{G}} = \underline{U} \cdot \underline{\underline{G}} \cdot \underline{\underline{P}} \qquad (9)$$

where $P_{ij} = r_i G_{ij}$

This equation is a recursion relation to be used with each successive reflection. Thus successive application of this recursion relation to equation (8) yields the expression after n reflections

$$\underline{U} = (\underline{a} + \underline{t}) \cdot \underline{\underline{G}} \cdot \left(\sum_{i=1}^{n-1} \underline{\underline{P}}^{(n)}\right) + \underline{U} \cdot \underline{\underline{G}} \cdot \underline{\underline{P}}^{(n)} \qquad (10)$$

where $\underline{\underline{P}}^{(n)} = \underline{\underline{P}} \cdot \underline{\underline{P}} \cdot \underline{\underline{P}} \cdots \underline{\underline{P}}$ (n-times)

Again, the second term represents what remains of the radiation field after n reflections. Since the components of both $\underline{\underline{G}}$ and $\underline{\underline{P}}$ are less than 1, the remainder becomes smaller as the number of reflections increases. In the limit of infinite reflections the second term vanishes and the series in the first term converges to the matrix $\underline{\underline{S}}$ such that

$$\underline{\underline{S}} = \underline{\underline{I}} + \underline{\underline{P}} + \underline{\underline{P}} \cdot \underline{\underline{P}} + \text{----} = (\underline{\underline{I}} - \underline{\underline{P}})^{-1} \qquad (11)$$

where $\underline{\underline{I}}$ is the unit matrix. Thus, equation 6 can be recast into the form:

$$\underline{U} = (\underline{a} + \underline{t}) \cdot \underline{\underline{J}} \qquad (12)$$

where the illumination tensor $\underline{\underline{J}}$ is given by

$$\underline{\underline{J}} = \underline{\underline{G}} \cdot \underline{\underline{S}} \qquad (13)$$

The physical interpretation of the component J_{ij} is that it is the fraction of the radiation from surface j that arrives at surface i after all the reflections have been accounted for.

Multi-Space

If we now extend our family of surfaces beyond a single enclosed volume to include other volumes that may be connected through transparent walls, and even to include the outside we can develop a more generalized illumination tensor. The sky can be treated as an all enclosing vault. At present DEROB does not treat the sky in this manner.

The second term in the right hand side of equation 12 can be rewritten in the form

$$\underline{t} \cdot \underline{\underline{J}} = (\underline{a} + \underline{t}) \cdot \underline{\underline{J}} \cdot \underline{\underline{H}} \qquad (14)$$

where $\underline{\underline{H}}$ is defined by the sum of the direct products

$$\underline{\underline{H}} = \sum_i (\underline{e}_k)\ (t_i \underline{\underline{e}}_i \cdot \underline{\underline{J}}) \qquad (15)$$

where $t_i \underline{\underline{e}}_i \cdot \underline{\underline{J}}$ is a row vector and $\underline{e}_j$ is the jth base vector. The indecis i and k represent the surface numbers of either side of the transparent wall and they are related by the bookkeeping scheme described earlier. The radiation comes from the ith side into the kth side so that the kth side can now be considered as an extended source of radiation.

Equation 14 is the transmittance recursion relation which is applied repeatedly to equation 13 to obtain another infinite series that converges to the form

$$\underline{\underline{T}} = \underline{\underline{I}} + \underline{\underline{H}} + \underline{\underline{H}} \cdot \underline{\underline{H}} + \text{----} = (\underline{\underline{I}} - \underline{\underline{H}})^{-1} \qquad (16)$$

so that equation 13 reduces to

$$\underline{U} = \underline{a} \cdot \underline{\underline{F}} \qquad (17)$$

where the generalized illumination tensor is defined by the product

$$\underline{\underline{F}} = \underline{\underline{J}} \cdot \underline{\underline{T}} \qquad (18)$$

The component F_{ij} gives the fraction of all the radiation originated on surface j that arrives on surface i and is ready for absorption after all the multiple reflections and transmissions have been taken into account. For the special case where the sky-vault and the external objects are not treated as members of this set of surfaces the sum of equation 15 should exclude all external transparent surfaces.[4]

[4] The present version of DEROB runs with this limitation.